

Channeling effects observed in energy-loss spectra of nitrogen ions scattered off a Pt(110) surface

A. Robin* and W. Heiland

Universität Osnabrück, D-49069 Osnabrück, Germany

J. Jensen

Manne Siegbahn Laboratory, S-104 05 Stockholm, Sweden

J. I. Juaristi and A. Arnau

Departamento de Física de Materiales, Facultad de Químicas, Universidad del País Vasco, Apartado 1072, E-20080, San Sebastian, Spain

(Received 6 June 2001; published 2 October 2001)

We present measured energy-loss spectra of nitrogen ions, which are scattered off a (1×2) missing row reconstructed Pt(110) single-crystal surface. The primary energy is varied from below 1 keV up to above 1 MeV, i.e., $0.04v_0 < v < 2v_0$ with v_0 the *Bohr velocity*. We use grazing angles low enough in order to have surface channeling at all energies. Experimental results are compared with theoretical energy-loss values obtained from trajectory and stopping power calculations of charged particles scattered under grazing incidence conditions from metallic surfaces. The stopping power is calculated using the scattering theory formalism. Different trajectory classes are found by the calculations and assigned to different contributions in the energy-loss spectra. Regarding the simplicity of the presented model the agreement with the experiment is good.

DOI: 10.1103/PhysRevA.64.052901

PACS number(s): 34.50.Bw, 34.50.Dy, 61.85.+p, 79.20.Rf

I. INTRODUCTION

During the last decades, many experiments have been performed with charged particles penetrating bulk matter (see [1] and references therein). In many of these experiments, the stopping power can be calculated by dividing the measured energy loss of the projectiles by their trajectory length, which is given by the target thickness. Two parts contribute to the energy loss of charged particles interacting with matter. The nuclear losses are of elastic nature and can be calculated from binary collision models. The electronic losses, which are mainly inelastic, are more difficult to describe. To do so, detailed knowledge of projectile and target properties is needed.

In the case of surface scattering, the situation is even more complicated. The impact parameters are not limited by the target density, hence, effects taking place 10–20 a.u. in front of the surface may contribute to energy losses. The trajectory lengths are difficult to define and depend on the scattering conditions, like angle of incidence and azimuthal angle. Therefore, the surface structure has a strong influence on the interaction by determining the trajectories of the projectiles. Surface energy-loss experiments are possible only with a single-crystal surface. Polycrystalline or amorphous material surfaces cannot be prepared in a controlled way. Therefore, in surface energy-loss experiments, we always deal with channeling.

In the present paper, we investigate the influence of the surface structure on the projectiles trajectories and the way this affects the energy loss of nitrogen ions that are scattered under grazing incidence along defined crystalline directions off a Pt(110)/ (1×2) reconstructed single-crystal surface.

The results of the experiments are compared with theoretical energy-loss values, which are calculated using the transport cross section at the Fermi level using a self-consistent scattering potential obtained in density-functional theory (DFT) as applied to a static impurity in jellium [2].

We present experimental data for N^+ ions from below 1 to 10 keV, N^{5+} ions at 75 keV and N^+ ions in the 1 MeV range. In Table I, the experimental conditions are shown. Also, the elastic energy losses for single binary collisions between N and Pt are calculated using energy and momentum conservation [3]. The obtained elastic losses are of the order of a few eV, which is rather small compared with the experimental total-energy losses. Furthermore, in the case of small angles of incidence, multiple scattering or channeling occurs. Then, the elastic losses are below the single binary collision energy loss [3]. The elastic losses given in Table I can therefore be considered as upper limits. Consequently, the measured energy losses can be considered to be mainly due to inelastic processes involving electronic effects.

The low-energy experiments were done with the LLOKI setup at the University of Osnabrück [4], the middle-energy-range measurements with the electron cyclotron resonance (ECR) source at the Hahn-Meitner-Institute (HMI) in Berlin [5] and the high-energy experiments with the pelletron accelerator at the MPI für Metallforschung in Stuttgart [6].

The following section describes the different experimental setups. Next, the theoretical aspects are presented. Finally, the results of the model calculations will be compared with experimental data and discussed.

II. EXPERIMENT

We vary the primary energy of the ions, the primary charge state of the ions, and the (grazing) angle of incidence ψ . The target is Pt(110) in all cases. We always use a specu-

*Email address: arobin@uos.de

TABLE I. Overview of the experimental conditions: For all measurements, the primary energy E_0 , the angle of incidence ψ , the primary charge state q_{in} , the perpendicular component of the primary energy E_{\perp} , and the elastic energy loss $\Delta E^{elastic}$ are given. The outgoing charge states q_{out} are 0 for E_0 below 10 keV and +1 for $E_0 > 10$ keV.

E_0 (keV)	ψ (deg)	q_{in}	E_{\perp} (eV)	$\Delta E^{elastic}$ (eV)
0.77	3.1	1	2.3	0.6
1.06	3.1	1	3.1	0.9
1.30	3.1	1	3.8	1.1
2.06	3.1–6.1	1	6.023.3	1.7–6.8
3.06	3.1	1	8.9	2.6
4.07	3.1	1	11.9	3.4
4.48	2.1–5.1	1	6.1–35.4	1.8–10.1
6.13	3.1	1	17.9	5.1
8.09	3.1	1	23.6	6.8
9.99	3.1	1	29.2	8.4
75.0	1	5	22.8	6.6
700.0	0.2	1	8.5	2.4
1000.0	0.2	1	12.1	3.5
1400.0	0.2	1	17.0	4.9

lar reflection geometry, i.e., $\theta = 2\psi$ with θ as scattering angle. The azimuthal alignment of the crystal surface is 10° off the $[1\bar{1}0]$ semichannel in all experiments described here, except the 4 keV azimuth series. The energy component perpendicular to the target surface is important for this type of experiment. It is calculated from $E_{\perp} = E_0 \sin^2 \psi$ with E_0 as the primary energy and ψ as the angle of incidence. If E_{\perp} is chosen too high, surface channeling fails and most of the projectiles penetrate into the bulk. An overview of the experimental conditions discussed in this paper is given in Table I. E_{\perp} varies from about 2 to 35 eV. Depending on the energy range and the charge state of the scattered particles, different kinds of analyzing systems and detectors are used (see Secs. II A, II B, and II C).

Different experimental energy spectra are shown in Fig. 1 for E_0 between 1 keV and 1 MeV. The 75 keV measurements

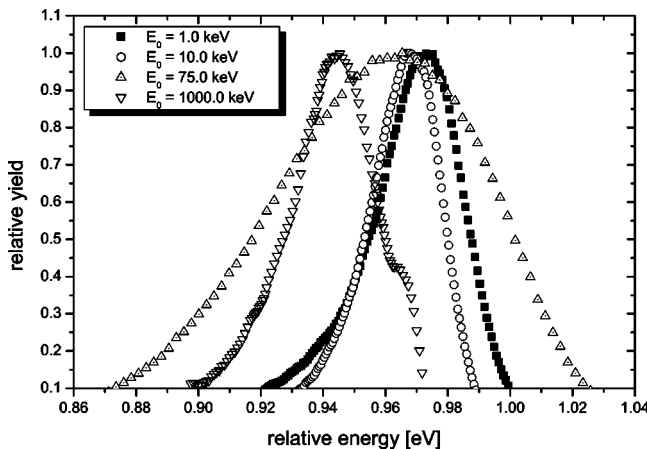


FIG. 1. Energy-loss spectra for different primary energies on a normalized scale. In all cases, specular reflection geometry is needed. Incoming angles ψ are adapted to surface channeling conditions (see Table I).

appear broadened. This is due to the detector resolution (see Sec. II B).

A. Low-energy range

Low-energy (0.7–10 keV) experiments are done at the LLOKI setup in Osnabrück with a basic chamber pressure of 3×10^{-10} mbar. An ATOMIKA ion source with a time of flight (TOF) measuring system is used, placed in forward direction to detect scattered particles under small scattering angles. The source can produce 1+ or 2+ charged ions. Since the beam intensity and quality is much better in the case of 1+ ions, we take N^+ as projectiles. The energy broadening of the primary beam is small [about 6 eV half width at half maximum in the 1 keV case] and the beam divergence in space is smaller than 0.3° , defined by a slit system.

Charged and neutral particles can be separated by a post-acceleration stage in the TOF tube. At the experimental conditions chosen, more than 99% of the scattered projectiles are neutralized after the scattering process. As detector, we use two multi channel plates (MCP's) of 32 mm diameter, situated 1558 mm downstream from the target. The detecting system has an acceptance angle of 1.2° and an energy resolution dE/E_0 of 1×10^{-3} . It can be rotated to change the scattering angle.

The target is prepared by scanning a 2 keV Ne^+ beam over the crystal surface. During the sputtering process, the target is heated up to 730 K. At the end, the target is annealed at 1050 K for typically 5 min. This preparing cycle is repeated several times to get a well-prepared (1×2) reconstructed surface.

Surface structure and quality is controlled by qualitative (visual) low-energy electron diffraction (LEED) and ion scattering spectroscopy (ISS). ISS gives chemical information about the remaining impurities at the surface. LEED also offers the possibility to adjust the crystalline azimuth within

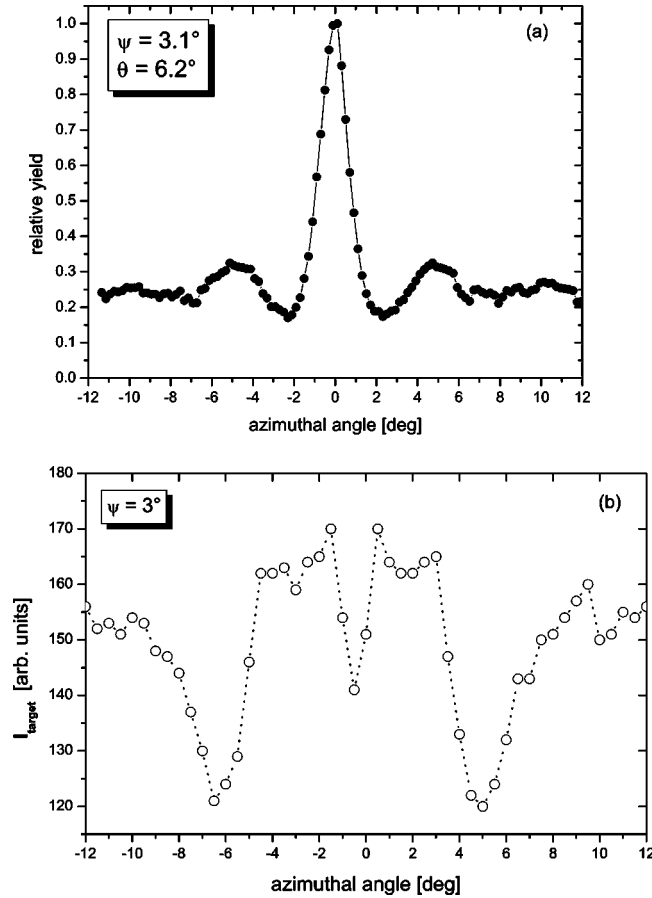


FIG. 2. Azimuthal scans of the Pt(110)(1 \times 2) reconstructed surface to adjust the $[1\bar{1}0]$ direction. (a) Scattered intensity of a 8 keV N^+ ion beam in forward direction (taken at the LLOKI setup in specular reflection geometry). The peak at 0° corresponds to the $[1\bar{1}0]$ semichannel. (b) Target current of a 1.4 MeV N^{2+} ion beam with an angle of incidence of 3° (Stuttgart). Lines are drawn to guide the eye.

an accuracy of $\pm 1^\circ$. Better accuracy is achieved by measuring the scattered intensity of the ion beam in the forward direction during an azimuthal scan. This allows a precision better than 0.5° for adjusting the $[1\bar{1}0]$ direction.

Figure 2(a) shows an azimuthal scan of 8090 eV N^+ ions scattered in specular reflection geometry off a (1 \times 2) reconstructed Pt(110) surface. The peak at $\phi=0^\circ$ indicates the surface channel in $[1\bar{1}0]$ direction. The symmetry of the spectrum reflects good quality of the target preparation and good adjustment. Figure 2(b) is from the 1 MeV experiment. Lines are drawn to guide the eye.

Energy-loss spectra with a variation of ψ are shown in Fig. 3 for two different values of E_0 . In (a) 2 keV measurements in specular reflection geometry are shown by varying ψ from 3.1° to 6.1° , i.e., a change in E_\perp from 6 to 23.3 eV. A continuous increase of ΔE with increasing ψ is shown. This is because we are below the critical perpendicular energy, so surface channeling holds on. Figure 3(b) shows a similar sequence of spectra for particles with a primary energy of 4.5 keV. In this case, E_\perp changes from 6.1 to 35.4 eV and no increase of ΔE is seen for $\psi > 4.1^\circ$ (see discussion).

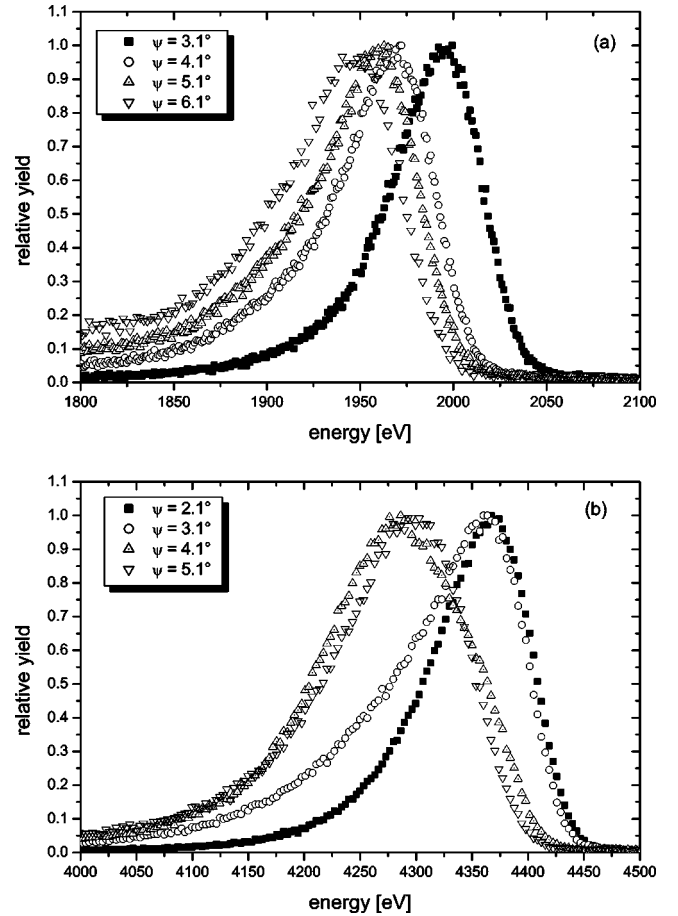


FIG. 3. Energy-loss spectra of N^+ ions scattered off a Pt(110)(1 \times 2) surface in specular reflection geometry. The azimuthal angle is $\phi=10^\circ$ in all cases. (a) 2 keV measurements with ψ varying from 3.1° to 6.1° , i.e., a change in E_\perp from 6 to 23.3 eV. ΔE increases continuously with ψ . (b) 4.5 keV spectra with ψ varying from 2.1° to 5.1° , i.e., a change in E_\perp from 6 to 35.4 eV. Increase of ΔE saturates for $\psi=5.1^\circ$.

B. Medium energy range

The 75 keV ions are produced by the 14.5 GHz electron cyclotron resonance (ECR) source at the HMI in Berlin [5]. With a maximum acceleration voltage of 15 kV, highly charged ions can be extracted. We use N^{5+} ions to have a maximum E_0 of 75 keV and to exclude effects from K -shell holes on the energy loss [7].

Ar^+ sputtering and annealing is used for cleaning the surface in the same manner as at the LLOKI setup. The sputtering gun provides a beam current in the μA range using 3 kV acceleration voltage. Structure control is done by LEED, which is also used for adjusting the target within an accuracy of $\pm 1^\circ$.

The detecting device consists of a collimator, an electrostatic analyzer (ESA) and a channeltron. The ESA detector was built in Osnabrück. The shape of the voltage plates is different, i.e., one is flat and the other parabolic. This enables a small detector size (136 \times 52 mm) and low voltages. With a target-detector distance of 32 mm and an aperture of 1 mm the acceptance angle results in 0.5° . The energy resolution of

the detector is determined by the slits of the collimator and those in front of the channeltron. In our case, we get a theoretical resolution of $dE/E_0 = 1.5 \times 10^{-2}$, which limits the accuracy of the energy-loss measurements (for details see [8]).

Most of the particles are neutralized after the scattering process [8,9]. We detect outgoing charge states from $q_{out} = 1+$ up to $q_{out} = 3+$. The yields of the higher-charge states ($q_{out} \geq 2+$) decrease drastically. Only values of scattered N^+ ions are taken for the energy loss discussion.

C. High-energy range

The experiments at the Max-Planck-Institute (MPI) in Stuttgart are obtained with a 6 MeV Pelletron accelerator [6] and a high-resolution electrostatic spectrometer [10]. Charge over mass separation is done by a 90° magnet. Magnetic lens systems in combination with slits, focus and confine the beam. The detecting system, combining an ESA and a MCP with a resistive anode for position analysis of the detected particles, has a maximum energy resolution dE/E_0 of 3×10^{-4} . The experimental resolution used in our experiments is $dE/E_0 = 5 \times 10^{-4}$ [10]. Note that due to charge-exchange processes, the primary charge state is not preserved during scattering. Outgoing charge states up to N^{6+} are detected. The average outgoing charge state is approximately 2.2 depending on the primary energy. A typical spectrum of the raw data of a 1.0 MeV N^+ surface channeling experiment off Pt(110) is published elsewhere [11]. For the energy-loss discussion, the values of the outgoing N^+ ions are taken.

The target is cleaned by sputtering and annealing. The structure is controlled using LEED, as in the experiments in Osnabrück and Berlin. Adjustment of the angle of incidence is done by a laser beam. The azimuth is adjusted by measuring the target current during an azimuthal scan. That gives a precision better than 0.3° for adjusting the $[1\bar{1}0]$ directions. Figure 2(b) shows an azimuthal target current scanning 1400 keV N^{2+} ions at $\psi = 3^\circ$. As in Fig. 2(a), the good symmetry indicates a well-prepared and well-adjusted surface. The minimum at $\phi = 0^\circ$ defines the $[1\bar{1}0]$ direction.

D. The Pt(110) crystal

We studied the Pt(110) surface previously with scanning tunneling microscopy (STM) and low-energy ion scattering [12,13]. The clean Pt(110) crystal forms a (1×2) missing row structure, i.e., every other $[1\bar{1}0]$ chain is missing and wide surface semichannels are formed. Mesoscopically, a fish-scale pattern is formed with elongated terraces of rhomboidal shape. They have average lengths of 50–60 nm along the $[1\bar{1}0]$ direction and a width of about 20 nm, i.e., the terraces are on average longer than the trajectories occurring in our experiments.

III. THEORETICAL ASPECTS

The energy loss ΔE is approximated by

$$\Delta E = L \frac{dE}{ds}, \quad (1)$$

where dE/ds characterizes the inelastic energy loss per unit length (stopping power) and L the interaction length, i.e., the part of the trajectory in which the ion interacts efficiently with the valence electrons of the metal surface [14,15]. Nuclear stopping processes are neglected. The transport cross section at the Fermi level $\sigma_{tr}(v_F)$ is related to the stopping power (dE/ds) of the ions ($v < v_F$) by

$$\frac{dE}{ds} = n_0 v v_F \sigma_{tr}(v_F) = v \gamma(Z_1, v_F), \quad (2)$$

where $v_F = (3\pi^2 n_0)^{1/3}$ is the Fermi velocity, n_0 the electronic density, $\gamma(Z_1, v_F)$ is the so-called friction coefficient and v the particle velocity that is taken as constant during interaction time. The transport cross section is calculated from a full phase-shift calculation of electron scattering in the self-consistent screened potential, calculated in density functional theory (DFT) [2]. The free-electron radius r_s is determined from EEL (electron energy loss) spectra to $r_s = 1.63$ a.u. [16]. This leads to $\gamma(v_F) = 1.44$ a.u. as the friction coefficient for the interaction of nitrogen particles in platinum.

The trajectory length L is computed from a Monte Carlo code using the Ziegler-Biersack-Littmark (ZBL) potential [1]. The code calculates at every trajectory point the sum of all potentials of the atoms within a certain area, i.e., the code creates a three dimensional box, following the actual point of the trajectories. The gradient of the potential gives the force acting on the projectile. By using this force, Newtons equations of motion are solved numerically. Thermal vibrations are included by calculating random displacements of the target atoms with a surface Debye temperature according to the Debye model. In a first step, the bulk value of 240 K is taken for all three dimensions.

For analyzing the trajectory length, it is necessary to define a z value as a starting point of the trajectory. This cutting edge z_{edge} limits the interaction distance of the projectiles related to energy-loss processes above the surface. The energy loss of the particles outside the limit of z_{edge} is estimated to be in the range of a few electron volts [17].

We take all the trajectories into account, which hit the detector after the scattering process. The size of the detector is equal to the experimental aperture of the detecting system. Different classes of trajectories are obtained and the inelastic energy losses ΔE of the respective projectiles are calculated from Eqs. (1) and (2).

Further information obtained from the trajectory calculation are the percentage of particles hitting the detector, the average length L , and the turning point z_0 of the trajectories with respect to the atom positions of the surface. Going to lower primary energies and smaller incident angles increases z_0 and shortens the trajectory lengths.

IV. RESULTS AND DISCUSSION

The experimental energy loss is given by the difference between the maximum of the measured energy distribution of the scattered particles and the primary energy E_0 .

We start the energy-loss calculation with an approximated value for the limit of the interaction zone z_{edge} . The starting value is $z_{edge} = 2.2$ a.u.

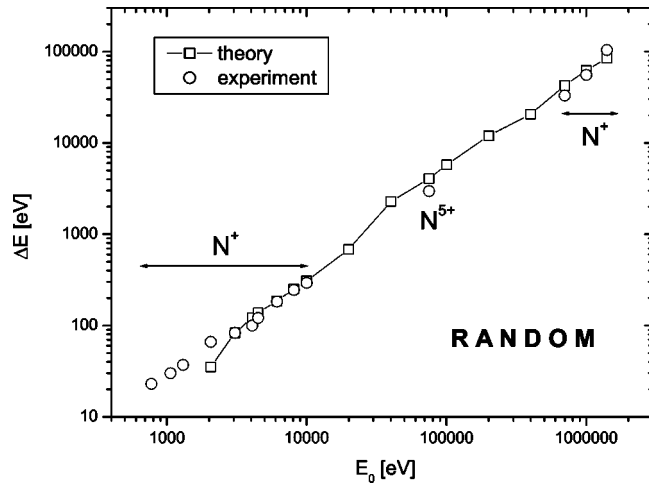


FIG. 4. Comparison of experimental energy losses with theoretical values for $z_{edge}=2.6$ a.u. For $E_0 > 2$ keV, the theory fits the experiment qualitatively. The scattering geometry is listed in Table I. Labels indicate the incoming charge states, respectively. Lines are drawn to guide the eye.

With the so-defined z_{edge} , we calculate average projectile trajectory lengths L for the different geometries and primary energies. Using $\gamma_r(v_F) = 1.44$ a.u. in Eq. (1) we estimate a theoretical energy loss. The calculated energy losses are fitted to the experimental data by optimizing the cutting limit z_{edge} . The parameter z_{edge} can be understood as a target property depending on the azimuthal direction because of corrugation effects. If z_{edge} is a target property indeed, it should be possible to find *one* z_{edge} that leads to good agreement with all experimental energy losses.

With $z_{edge} = 2.6$ a.u., we get the best agreement for primary energies from above 2 to 10 keV (Fig. 4). The theoretical values are in good agreement with the experimental data over a primary energy range of three decades.

Deviations between experiment and theory are more clearly seen in Fig. 5 using a linear scale. At the low energy end, i.e., $E_0 \leq 2$ keV, the theoretical values are below the experiment. This is due to the fact that at 2 keV and $\psi = 3.1^\circ$, i.e., $E_\perp = 6$ eV, the turning point z_0 of the trajectories is in the region of z_{edge} , i.e., the calculated L is very small (Fig. 6). The model with the z_{edge} value used predicts

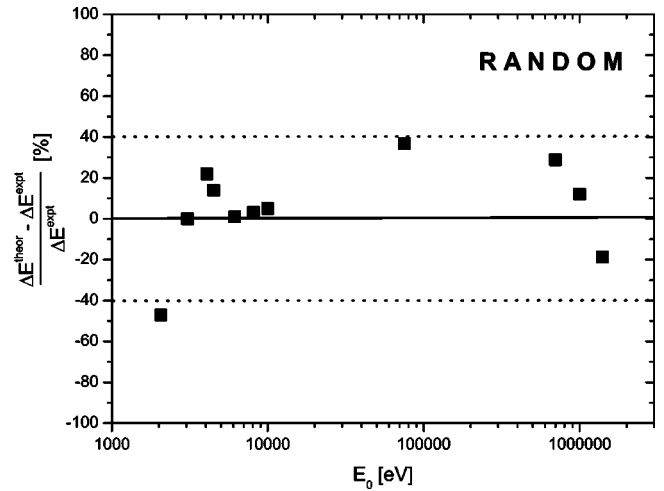


FIG. 5. Difference between theoretical and experimental energy loss relative to the experimental value. From $E_0 = 2$ keV onwards the agreement is better than 40%.

essentially no energy loss in the case of very low energies or very grazing incidence, i.e., $E_\perp < 5$ eV. Long-distance effects resulting from the Coulomb interaction are neglected in the calculation. Hence, the obtained energy-loss values are lower than the experimental losses.

Figure 4 shows a linear relation between primary energy and energy loss. This reflects the linear dependence of the stopping power on the velocity and an approximately linear increase of L with increasing velocity [17]. The L dependency on velocity only is observed, if E_\perp remains below a critical value. Nürmann *et al.* found in the case of H^+ ions interacting with a Ni(110) surface, that L saturates for E_\perp larger than a critical value of 37 eV [17]. Particles with higher E_\perp penetrate the first layers and probe the bulk properties. Experimentally, we have at least two possibilities to verify this assumption. Firstly, by increasing the primary energy, i.e., using projectiles with, e.g., $E_0 > 12.7$ keV and secondly, by changing the incident angle, e.g., taking 4.5 keV ions with $\psi = 5.1^\circ$ or more. Figure 3(b) provides evidence for our assumption.

In the case of $\psi = 5.1^\circ$, we exit the regime of surface channeling, i.e., trajectory lengths saturate. This can be seen in the spectra as well, if one looks at the missing increase in

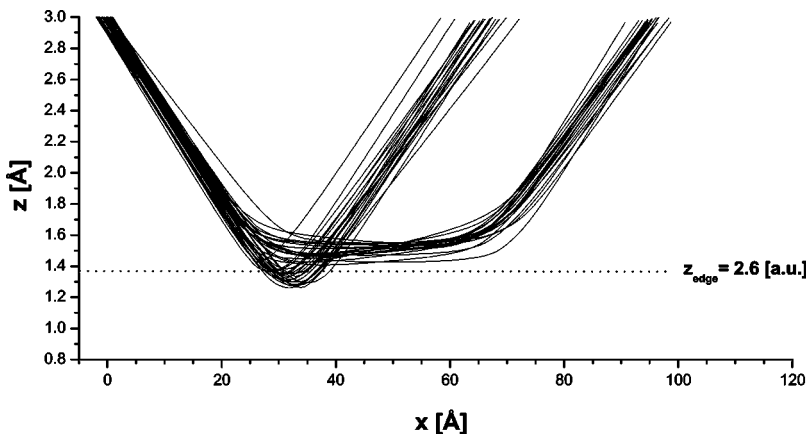


FIG. 6. Trajectory calculations for 2 keV N^+ ions scattering off Pt(110)(1 \times 2) with $\psi = 3.1^\circ$ and $\phi = 10^\circ$. The perpendicular part of the energy is $E_\perp = 6$ eV. Trajectories' turning point is in the range of z_{edge} .

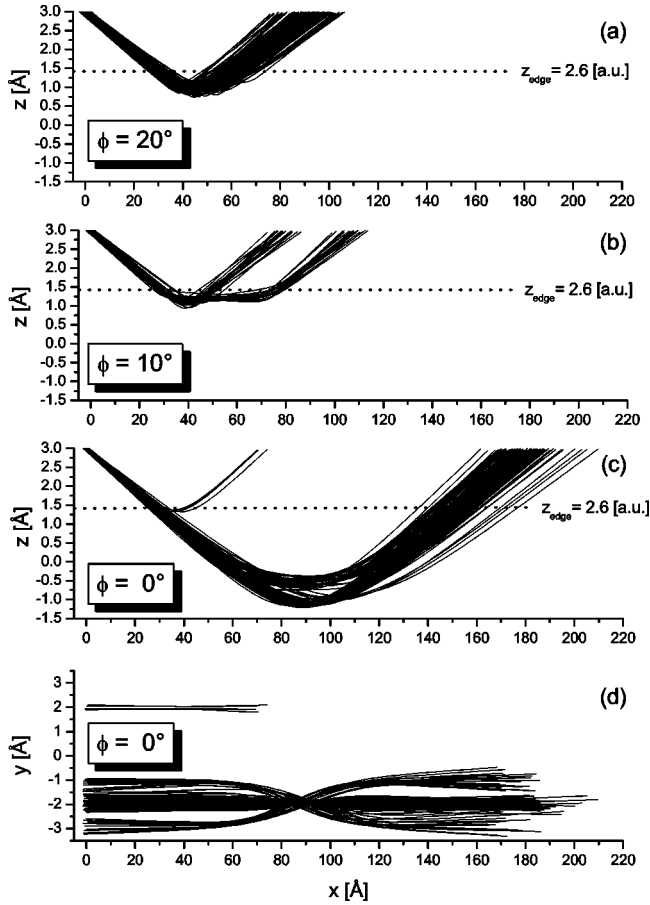


FIG. 7. Trajectories for 4.5 keV N^+ ions scattering off Pt(110)(1 \times 2) with $\psi=3.1^\circ$. (a)–(c) show a side view of the trajectories. ϕ is varied from (a) 20° over (b) 10° to (c) 0° . The development of the *in-channel* class (long trajectories) is clearly seen. (d) shows a top view of (c). Three classes of trajectories can be distinguished (*short*, *long*, and *zigzag*).

energy loss for the $\psi=5.1^\circ$ data. In consequence, we expect a stop in the increase of the average trajectory length with increasing ψ to reflect the energy-loss behavior.

We made a detailed analysis of a large number of calculated trajectories for our range of experiments. The simulations were done for $\phi=0^\circ$, the $[1\bar{1}0]$ channel, and for $\phi=10^\circ$ and $\phi=20^\circ$ off the $[1\bar{1}0]$ direction. We find two different classes of trajectories.

(i) hyperbolic-shaped trajectories, which are typical for planar channeling; in the following, we will call them the *short* trajectories.

(ii) very flat, stretched trajectories with a special steering in the $[1\bar{1}0]$ channel. These ions move for more than 70 a.u. parallel to the surface. In the following, we call them the *long* trajectories.

For scattering along the $[1\bar{1}0]$ channel, the long trajectories are dominant. At $\phi=20^\circ$ only short trajectories prevail. Simulations with azimuthal angles from $\phi=0^\circ$ to 20° show a transition of the long trajectories into the short trajectories. The average distance of the turning point z_0

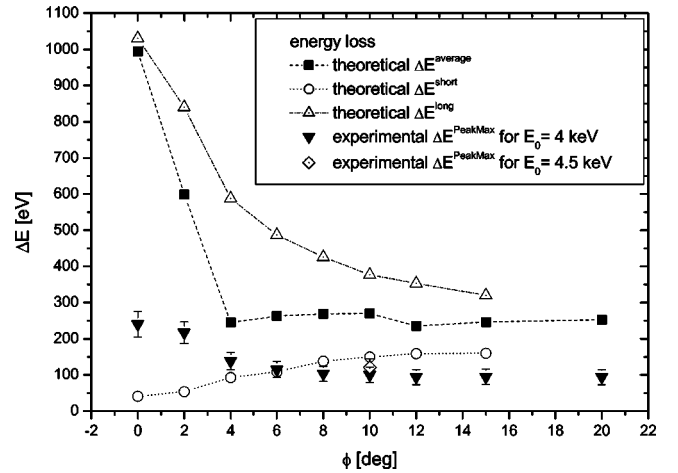
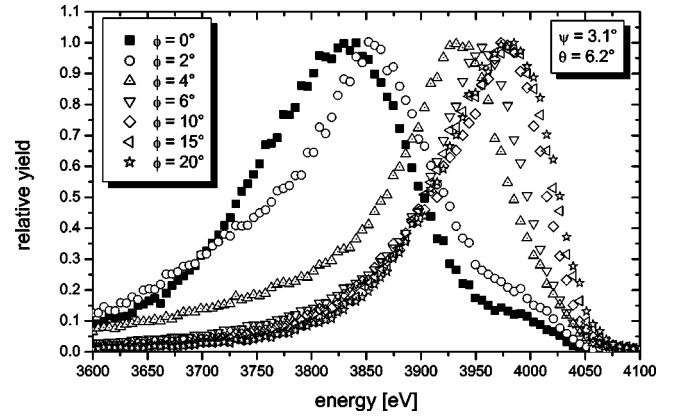


FIG. 8. Azimuthal series of energy-loss data for N^+ ions scattered off a Pt(110)(1 \times 2) surface with an angle of incidence of $\psi=3.1^\circ$. (a) Energy-loss spectra for $E_0=4$ keV. The peak position shifts to higher energies with increasing ϕ . The spectra in the $[1\bar{1}0]$ channel is broadened. (b) Theoretical energy losses of 4.5 keV N^+ ions. Values are shown for short and long trajectories as well as for the average losses. In addition, we show experimental values of the peak maximum for 4 and 4.5 keV. Lines are drawn to guide the eye.

related to the first atomic layer of the target decreases with increasing ϕ (Fig. 7).

The existence of the two trajectory classes is not obvious when looking at the experimental energy spectra. In Fig. 8(a) spectra from $\phi=0^\circ$ to 20° are shown for a primary energy of 4 keV, $\psi=3.1^\circ$ and $\theta=6.2^\circ$. There is no evidence from the peak shape for two energy-loss distributions as predicted by the calculations for the case of $\phi=10^\circ$. Also, the maximum peak position is independent of ϕ for $\phi\geq 6^\circ$. These findings are explained by calculating the average energy losses, which are obtained by weighting the energy losses of the short and the long trajectories with their respective intensities.

As shown in Fig. 8(b), the calculated average energy losses are independent of ϕ for $\phi\geq 4^\circ$, too. The energy loss of the short trajectories increases with ϕ , whereas the energy loss of the long trajectories decreases with ϕ . The findings for the average energy loss agree with the experimental data. Note that the experimental values are shown for

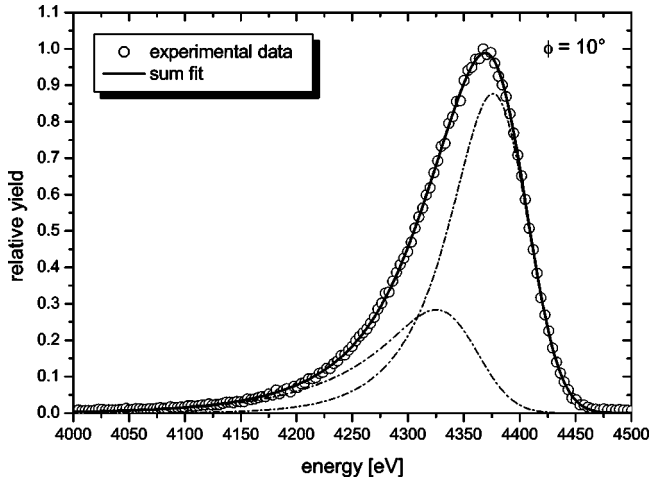


FIG. 9. Two-function fit to an experimental spectrum for $E_0 = 4.5$ keV and $\psi = 2.1^\circ$.

$E_0 = 4$ keV, the theoretical values for $E_0 = 4.5$ keV. Together with an overestimation of the contribution of the long trajectories, the difference in the absolute values can be explained.

Close to the channel, the theoretical values for the average energy loss are significantly higher than the experimental ones [Fig. 8(a) for $\phi = 0^\circ, 2^\circ$]. Hence, an influence of the surface corrugation on z_{edge} has to be considered. Comparing the experimental spectra for $\phi = 0^\circ, 10^\circ$ from Fig. 8, it is evident, that the small intensity peak at the high-energy side of the distribution develops in the main peak of the $\phi = 10^\circ$ spectra. Explaining this by the trajectory picture means that these contributions result from the same class of trajectories, namely, the short ones scattered planar from the surface. Details of the *in-channel* spectra will be discussed in a forthcoming paper.

To get a clue of how strong the long trajectories contribute, we fit the experimental data with two instead of one energy-distribution functions corresponding to the two trajectory classes. Therefore, we use typical energy-loss-type function, i.e., a Gaussian function convoluted with an exponential decay function as proposed by Nürmann [4,18]. With two fit functions, the agreement of the fit with the experiment is improved. In most cases, it is indeed necessary to take a second fit function to reach agreement.

From Fig. 9, it can be deduced that one function mainly fits the peak of the energy-loss distribution, whereas the other one fits the broadened low-energy shoulder of the peak. Because of the higher mean-energy loss of the latter one, we assume that this contribution describes the long trajectories whereas the narrow distribution represents the short trajectories. This assumption is supported by the fact that the broadening of the function representing the long trajectories can be explained by the results of the trajectory simulations. Since the depth distribution in z direction is much smaller in the case of the short trajectories compared with the long ones, the resulting length distribution is broadened for the latter. In consequence, the electron density felt by the projectiles differs more in case of the long trajectories that lead to a broadening of the energy-loss distribution, too. Small variations of

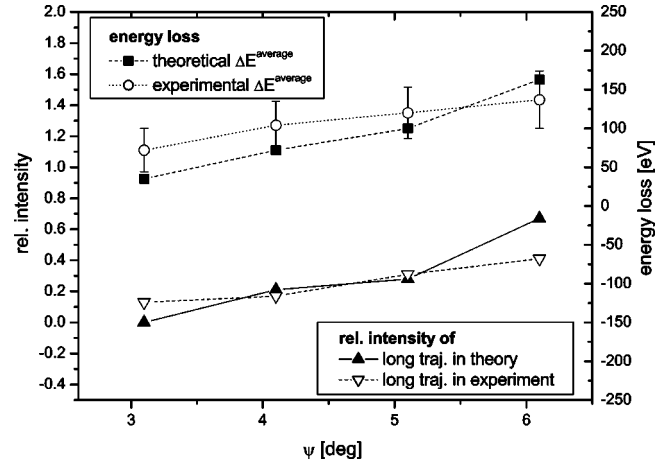


FIG. 10. Comparison of experiment and theory for varied ψ in case of $E_0 = 2$ keV and $\phi = 10^\circ$.

the fit parameters show that the relation between the intensities of the two functions changes significantly, whereas the energy position of the peak maximum is almost unchanged. But in the case of $E_0 = 2$ keV, the percentage of long trajectories also fits well (Fig. 10).

What kind of conclusions can be made from these findings concerning the energy-loss dependency on ψ for the 2 and 4.5 keV measurements? As shown in Fig. 10, the agreement between theory and experiment increases with ψ for the 2 keV measurements. From $\psi = 4.1^\circ$ onwards, the average calculated energy loss fits in the limit of the error bars the experimental energy loss well. Also, the more or less linear increase with ψ is well described by the theory.

In the case of 4.5 keV, the agreement between theory and experiment is not as good as at 2 keV (Fig. 11). The increase of the average energy loss with ψ becomes overestimated by the theory for $\psi > 3^\circ$. The reason has to be an overestimation of the influence of the long trajectories, because the agreement between theory and experiment for the short trajectories is good (Fig. 11). Note the short trajectories represent the

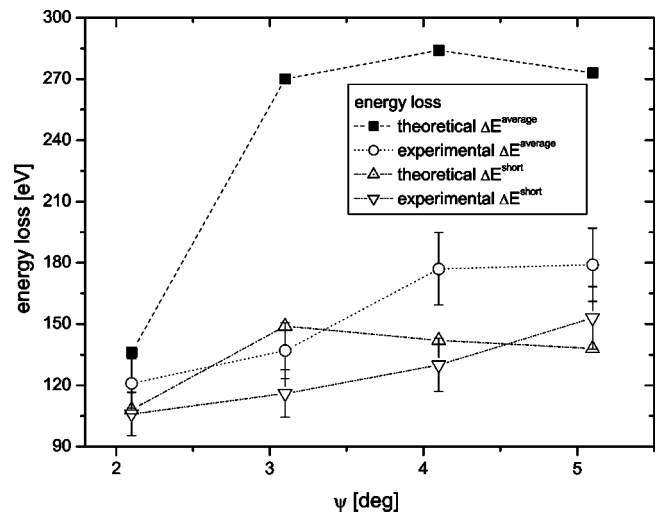


FIG. 11. Comparison of experimental and theoretical energy losses for varying ψ in case of $E_0 = 4.5$ keV and $\phi = 10^\circ$.

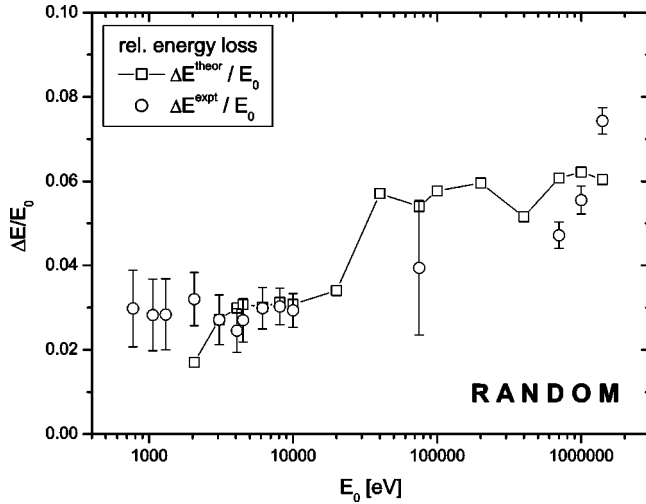


FIG. 12. Comparison of the relative energy loss $\Delta E/E_0$. Error bars indicate the experimental uncertainty.

planar channeled particles. The long trajectories represent particles following surface semichannels. This gives calculated values for the length of $L=44$ a.u. in the case of $\psi=2.1^\circ$ and $L=80-90$ a.u. for $\psi>3^\circ$, i.e., up to three times higher than for the short trajectories ($L=25-33$ a.u.). In the calculation, both trajectory classes contribute around 50%.

Having in mind that a real surface always contains steps and impurities, the percentage of ions following these long trajectories may be overestimated by the computer calculations, especially for $\psi>3^\circ$. But the experimental finding of the general behavior of the average energy-loss dependence on ψ , which is an increase up to around $\psi=4^\circ$, followed by a saturation, is well explained by the theory for the 4.5 keV data, too.

For a further understanding of the channeling behavior, we varied the target Debye temperature in the trajectory calculations. At lower Debye temperatures, the thermal vibrational amplitudes of the atoms increase. The increased thermal amplitudes cause a decrease of the effect of surface semichannels. But also for $T_{Debye}=120$ K, i.e., half of the bulk value, we get qualitatively the same results. The total number of particles hitting the detector is lowered by 30–40%, i.e., the scattering becomes more “diffuse.” The distribution of the trajectory lengths broadens, causing a broadening of the calculated energy distribution, too. The relative contributions of long and short trajectories to the total do not change significantly. These findings strengthen the conclusion that a careful trajectory analysis is needed for the analysis of experimental energy-loss spectra. In our case, the width of the energy-loss spectra is caused to a large extent by trajectory effects and not so much by energy-loss straggling. Besides the thermal vibrational amplitude of the target atoms, the quality of the surface influences the characteristics of the trajectory distribution. As we know from STM [12], the surface of Pt(110) forms the so-called fish-scale pattern, i.e., there are steps according to the average terrace length of 25 nm in the $\phi=10^\circ$ direction. Together with other defects, this may lead to an overestimation of the long-guided trajectories in the calculations. The average length of the long

trajectories is, e.g., 5 nm for $E_0=4.5$ keV, the length of the short trajectories is less than 2 nm. This argument is supported by the fact that Fig. 11 shows the best overall agreement between the average experimental energy loss and the calculated value for the short trajectories (see also Figs. 4 and 5).

In the 1 MeV region, the experimental energy losses show small deviations from the linear dependency with E_0 (Fig. 12). The super-proportional increase is due to charge-exchange processes, which occur during the scattering interaction. The ions are not neutral in front of the surface (as in the <10 keV range), but interact as charged particles with the surface. The interaction time is estimated long enough to form an equilibrium charge state in the range between +2 and +3 [11]. The additional charge-exchange processes contribute in two ways to the energy loss. First, the stopping is stronger for charged particles compared with the stopping for neutrals—the stopping is approximately proportional to the square of the charge state at high velocities, and a more complicated dependence has been found at lower velocities [7,14]—and second, the charge exchange itself contributes to the energy loss. Experimentally, this increase of the energy loss is significant, as shown in Fig. 12.

Since our theory does not take into account charge-exchange effects, it cannot describe this additional energy loss for $E_0>700$ keV. To consider these influences, we have to know more about the transition rates between the different charge states. Knowing them, we can calculate an average number of charge-exchange processes, which occur during projectile-surface interaction. This gives us different interaction lengths L^q for every possible charge state q [14]. The sum over L^q with $q=1,2,\dots,7$ has to give L . With this kind of improvements, it should be possible to include the effects of charge exchange in our model [17].

The two kinds of trajectory classes from Fig. 7 can be seen in the 0.7–1.4 MeV energy regime, too. The effect on the calculated energy loss is small, approximately 2–4 keV, because the length difference between the two classes is negligible compared to the low-energy regime. The smaller shadow cone prevents the projectiles to follow any special surface channel.

V. CONCLUSION

In summary, we have calculated in this paper, energy loss of nitrogen ions scattered off a Pt(110) surface. The obtained values are in good agreement with the maximum peak position in the measured energy-loss spectra for the presented primary energy range. For the whole range of experiments, only one “fit” parameter z_{edge} is used for the theoretical description with one numerical value $z_{edge}=2.6$ a.u.. By defining the interaction zone by $z_{edge}=2.6$ a.u., we well describe experiments with $E_\perp\geq 10$ eV. Because the theoretical model does not include any charge-exchange processes, the calculated energy-loss values increase less than the experimental losses in the case of $E_0\geq 1$ MeV.

Furthermore, we find in the low-energy regime a split of the trajectories into two classes, long and short. The long trajectories cause a significant broadening of energy spectra. The comparison of calculated and experimental energy losses indicates an overestimation of the energy loss caused by the *long* trajectories.

In theory, this can be corrected by lowering the value for the edge, z_{edge} , or by decreasing the friction coefficient γ . Smaller γ values could indicate a lower z electron density inside the surface channel. Experimentally, long trajectories can be lost due to scattering at step edges.

In a forthcoming paper, we will discuss the results for scattering along the $[1\bar{1}0]$ direction, $\phi=0^\circ$, where three different trajectory classes have to be taken into account.

ACKNOWLEDGMENTS

This research was supported by the Deutsche Forschungsgemeinschaft (DFG). We thank D. Plachke, H. D. Carstanjen (MPI, Stuttgart), and D. Niemann (HMI, Berlin) for helpful discussions and generous support during the beam times. A.R. is thankful for the hospitality of the University of San Sebastian. J.J. acknowledges financial support from The Swedish Foundation for International Cooperation in Research and Higher Education (STINT) and the University of Osnabrück. J.I.I. and A.A. acknowledge partial support from the Spanish DGICYT (Project No. PB97-0636), Eusko Jauriaritza, Iberdrola S. A., Gipuzkoako Foru Aldundia, and Universidad del País Vasco.

-
- [1] J.F. Ziegler, J.P. Biersack, and U. Littmark, *The Stopping and Ranges of Ions in Matter* (Pergamon Press, New York, 1985), Vol. 1ff.
 - [2] P.M. Echenique, R.M. Nieminen, J.C. Ashley, and R.H. Ritchie, *Phys. Rev. A* **33**, 897 (1986).
 - [3] H. Niehus, W. Heiland, and E. Taglauer, *Surf. Sci. Rep.* **17**, 4 (1993).
 - [4] A. Nürmann, *On the Interaction of He Particles with Ni Surfaces* (Dissertations Druck, Darmstadt, 1989).
 - [5] B. Martin, M. Grether, R. Röhrbrück, U. Stettner, and H. Waldmann, *Proceedings of the 11th International Workshop on Electron Cyclotron Resonance Ion Sources (ECRIS 11)*, edited by A. G. Drentje, KVI Report No 996 (Groningen, The Netherlands, 1993).
 - [6] H.D. Carstanjen, W. Decker, and H. Stoll, *Z. Metallkd.* **84**, 368 (1993).
 - [7] J.I. Juaristi and A. Arnau, *Nucl. Instrum. Methods Phys. Res. B* **115**, 173 (1996).
 - [8] A. Arnau, F. Aumayr, P.M. Echenique, M. Grether, W. Heiland, J. Limburg, R. Morgenstern, P. Roncin, S. Schippers, R. Schuch, N. Stolterfoht, P. Varga, T.J.M. Zouros, and H.P. Winter, *Surf. Sci. Rep.* **27**, 4 (1997).
 - [9] L. Folkerts, S. Schippers, D.M. Zehner, and F.W. Meyer, *Phys. Rev. Lett.* **74**, 2204 (1995).
 - [10] H.D. Carstanjen, *Nucl. Instrum. Methods Phys. Res. B* **136**, 1183 (1998).
 - [11] A. Robin, N. Hatke, A. Nürmann, M. Grether, D. Plachke, J. Jensen, and W. Heiland, *Nucl. Instrum. Methods Phys. Res. B* **164**, 566 (2000).
 - [12] S. Speller, J. Kuntze, T. Rauch, J. Bömermann, M. Huck, M. Aschoff, and W. Heiland, *Surf. Sci.* **366**, 251 (1996).
 - [13] S. Speller, S. Parascandola, and W. Heiland, *Surf. Sci.* **383**, 131 (1997).
 - [14] J.I. Juaristi, A. Arnau, P.M. Echenique, C. Auth, and H. Winter, *Phys. Rev. Lett.* **82**, 1048 (1999); J.I. Juaristi, A. Arnau, P.M. Echenique, C. Auth, and H. Winter, *Nucl. Instrum. Methods Phys. Res. B* **157**, 87 (1999).
 - [15] J.I. Juaristi, C. Auth, H. Winter, A. Arnau, K. Eder, D. Semrad, F. Aumayr, P. Bauer, and P.M. Echenique, *Phys. Rev. Lett.* **84**, 2124 (2000).
 - [16] C. C. Ahn and O. L. Krivanek, R. P. Burgner, M. M. Disko, and P. R. Swann, *EELS Atlas, A Reference Guide of Electron Energy-Loss Spectra Covering all Stable Elements* (ASU, HREM Facility, 1983).
 - [17] A. Nürmann, W. Heiland, R. Monreal, F. Flores, and P.M. Echenique, *Phys. Rev. B* **44**, 2003 (1991).
 - [18] A. Nürmann, R. Monreal, P.M. Echenique, F. Flores, W. Heiland, and S. Schubert, *Phys. Rev. Lett.* **64**, 1601 (1990).